On the Generation of Large Passive Macromodels for Complex Interconnect Structures

On the Generation of Large Passive Macromodels for Complex Interconnect Structures

Stefano Grivet-Talocia, *Member, IEEE,* and Andrea Ubolli

***Abstract*—This paper addresses some issues related to the passivity of interconnect macromodels computed from measured or simulated port responses. The generation of such macromodels is usually performed via suitable least squares fitting algorithms. When the number of ports and the dynamic order of the macromodel is large, the inclusion of passivity constraints in the fitting process is cumbersome and results in excessive computational and storage requirements. Therefore, we consider in this work a post-processing approach for passivity enforcement, aimed at the detection and compensation of passivity violations without compromising the model accuracy. Two complementary issues are addressed. First, we consider the enforcement of asymptotic passivity at high frequencies based on the perturbation of the direct coupling term in the transfer matrix. We show how potential problems may arise when off-band poles are present in the model. Second, the enforcement of uniform passivity throughout the entire frequency axis is performed via an iterative perturbation scheme on the purely imaginary eigenvalues of associated Hamiltonian matrices. A special formulation of this spectral perturbation using possibly large but sparse matrices allows the passivity compensation to be performed at a cost which scales only linearly with the order of the system. This formulation involves a restarted Arnoldi iteration combined with a complex frequency hopping algorithm for the selective computation of the imaginary eigenvalues to be perturbed. Some examples of interconnect models are used to illustrate the performance of the proposed techniques.**

***Index Terms*—Admittance, Arnoldi algorithm, complex frequency hopping, eigenvalues, Hamiltonian matrices, hybrid, impedance, linear macromodeling, passivity, perturbation theory, scattering, singular values, sparse matrices.**

I. Introduction

THE ELECTRICAL design of high-speed information and communication systems requires accurate and efficient models for all critical components. In particular, the nonideal behavior of electrical interconnects and packaging structures at high frequency needs to be carefully taken into account to insure the signal integrity of the whole system. Therefore, much attention has been devoted in the literature to macromodel generation algorithms. Several techniques are available (see, e.g., [1]–[8]) for the construction of SPICE-ready macromodels starting from various forms of native characterization such as direct measurements or electromagnetic simulation, both in time and frequency domain. Most of these techniques lead to excellent results in terms of accuracy and efficiency when the structure under consideration has a limited port count and dynamic order. However, some difficulties arise when realistic structures such as connectors or via arrays are considered, since the port count that is needed to include all significant couplings may be quite large. Similarly, a possibly large dynamic order is required by the extended frequency band over which an accurate representation is necessary.

This paper addresses some difficulties that arise during the construction of large macromodels, both in terms of port count and dynamic order. Common macromodeling algorithms, such as vector fitting [8], are based on some least squares fitting to the data for the computation of the macromodel poles and residues. For a large macromodel, the whole transfer matrix cannot be fitted at the same time, since the resulting least squares system would require prohibitive computing time and storage. Therefore, a common approach is to fit separately subsets of port responses, and to collect them subsequently into a global macromodel [9], [10] (many commercial tools also use this approach). This strategy leads generally to excellent accuracy on each specific entry of the transfer matrix. Unfortunately, no control over macromodel passivity is possible, since passivity is a global feature of the transfer matrix and requires its consideration as a whole. Passivity is a fundamental property of any macromodel, since a nonpassive model may lead to unstable transient simulations depending on its termination networks [11], [12]. An illustrative example is included in this paper. Conversely, passive models guarantee stability under any termination condition [13], [14], thus insuring successful system-level simulations.

The main focus of this work is on the enforcement of passivity for a given large macromodel. Several techniques for passivity enforcement are available. The techniques proposed in [2] and [5] do not guarantee a passive macromodel although care is taken during its computation. Other approaches aimed at enforcing passivity by construction [15] may lead to overtreatment with significant loss of accuracy. Better solutions are based on formulation of passivity enforcement as the solution of linear and quadratic programming problems and, more generally, of convex optimization problems. Some of these techniques are based on passivity enforcement only at selected frequency points [16] and are, therefore, unable to guarantee passivity over the entire frequency spectrum. Some other techniques work directly on a state-space realization of the macromodel [17]–[19]. They do guarantee passivity, but their application is mainly limited by the problem size due to computational cost and storage requirements. The approach that we follow in this paper is based on the Hamiltonian matrix associated to the macromodel. Since passivity violations are

Manuscript received January 21, 2005; revised July 5, 2005. This work was supported in part by the Italian Ministry of Education, University and Research (MIUR) under a Program for the Development of Research of National Interest under PRIN Grant 2004093025.

The authors are with the Department of Electronics, Polytechnic of Turin, 10129 Turin, Italy (e-mail: grivet@polito.it).

Digital Object Identifier 10.1109/TADVP.2005.862659

implied by the existence of purely imaginary eigenvalues of the Hamiltonian matrix [20]–[22], we adopt an iterative perturbation scheme [21], [23] aimed at the direct displacement of these eigenvalues from the imaginary axis. This passivity enforcement scheme is based on the iterative determination of the eigenvalues of the Hamiltonian matrix, combined with the solution of small underdetermined linear least squares problems.

There are three main difficulties associated with this passivity enforcement scheme that arise when dealing with large macromodels. First, the algorithm assumes asymptotic passivity at high frequencies. However, this condition cannot be guaranteed if the macromodel is constructed in separate parts. Section III shows how asymptotic passivity can be enforced and highlights the conditions on the macromodel poles that need to be insured so that this procedure is numerically stable. The second difficulty is associated to the computation of the controllability Gramian of the macromodel. This is needed in order to guarantee preservation of accuracy throughout the iterations. However, the Gramian is computed by solving a Lyapunov equation [14], [24], which is well known to require considerable computational resources. Section IV shows that this is not an issue for the general class of macromodels that is considered in this paper, for which the Gramian is available analytically and results sparse and block-diagonal. The third and main difficulty is related to the actual computation of the Hamiltonian eigenvalues. Indeed, the associated computational cost scales as the third power of the problem size and becomes excessive for large macromodels. To overcome this problem, we employ here a restarted Arnoldi algorithm [25], [26] with shift-and-invert spectral transformation, combined with an iterative selection of multiple complex shifts similar to the well-known complex frequency hopping [27] algorithm. This results in an automatic algorithm that is capable of extracting all imaginary eigenvalues and associated eigenvectors with arbitrary precision. The resulting computational cost scales only linearly with the problem size, thus allowing applicability for large-sized macromodels. This eigenvalue computation algorithm is presented in Section V. Validations and numerical results are finally presented in Section VI.

II. Background and Notations

A. Sparse Macromodels

We consider a linear multiport structure with an arbitrary and possibly large number of ports P. The main objective of this paper is to check and enforce passivity of a macromodel of the structure, derived via some fitting algorithm such, e.g., vector fitting [8]. We assume that this macromodel is characterized by a rational transfer matrix expressed as

$$\boldsymbol{H}(s) = \boldsymbol{H}_\infty + \sum_{n=1}^{N} \frac{\boldsymbol{R}_n}{s - p_n}. \tag{1}$$

The most common representation for $\boldsymbol{H}(s)$ used for the construction of macromodels is the scattering form. We will consider in the following also hybrid representations, which include admittance and impedance as particular cases [13].

A common set of poles for all transfer matrix entries would be desirable under a theoretical standpoint. However, this condition requires the consideration of all responses at the same time in the derivation of the macromodel. Obviously, this is not possible when P is large, due to excessive storage and CPU time requirements. Therefore, a common approach is to fit separately subsets of port responses and to combine the results into a global macromodel. When this strategy is pushed to the limit, P^2 independent sets of poles and residues are obtained, one for each single transfer matrix entry. This choice optimizes speed and accuracy in the computation of the macromodel, but results into a very large number N of poles. In this paper, we follow a more general splitting strategy, which is outlined below. This strategy will lead to a state-space realization of (1) which results particularly convenient due to its sparsity pattern.

We assume that the complete set of P^2 port responses is denoted as

$$\Omega = \{(i,j), i,j = 1,\ldots,P\} \tag{2}$$

where (i,j) refers to the ith row and jth column of the transfer matrix $\boldsymbol{H}(s)$. This set is partitioned as

$$\Omega = \bigcup_k \Omega_k, \quad \bigcap_k \Omega_k = \emptyset \tag{3}$$

where

$$\Omega_k = \{(i_\nu, j_k), \nu = 1,\ldots,P_k\}. \tag{4}$$

Each subset Ω_k is, therefore, characterized by a fixed excitation (corresponding to the index j_k) and by multiple outputs indexed by i_ν. Note that in the particular case $P_k = P$ for all k, this corresponds to a columnwise partition of the transfer matrix, a common choice in the macromodeling literature [28]. It can be easily verified that the entire transfer matrix can be recovered as

$$\boldsymbol{H}(s) = \sum_{k=1}^{K} \boldsymbol{Q}_k^T \boldsymbol{H}_k(s) \boldsymbol{e}_{j_k}^T \tag{5}$$

where $\boldsymbol{H}_k(s)$ is the $P_k \times 1$ submatrix corresponding to Ω_k, i.e., part of column j_k of $\boldsymbol{H}(s)$, $\boldsymbol{e}_{j_k}$ is the j_kth Euclidean unit vector, and $\boldsymbol{Q}_k$ is a $P_k \times P$ port selector matrix having a single unitary entry in each row ν located at column i_ν, with all the other entries vanishing.

This splitting strategy allows to process independently all subsets in the generation of the rational approximation, leading to independent partial macromodels of the form

$$\boldsymbol{H}_k(s) \simeq \boldsymbol{H}_{k,\infty} + \sum_{n=1}^{N_k} \frac{\boldsymbol{R}_{k,n}}{s - p_{k,n}}. \tag{6}$$

A state-space realization for each $\boldsymbol{H}_k(s)$ is easily constructed. Denoting with u_k the single port excitation, with $\boldsymbol{y}_k$ the P_k outputs, and with $\boldsymbol{x}_k$ the state vector, we have

$$\begin{cases} \dot{\boldsymbol{x}}_k(t) = \boldsymbol{A}_k \boldsymbol{x}_k(t) + \boldsymbol{1}_{N_k} u_k(t) \\ \boldsymbol{y}_k(t) = \boldsymbol{C}_k \boldsymbol{x}_k(t) + \boldsymbol{D}_k u_k(t) \end{cases} \tag{7}$$

where $\boldsymbol{A}_k = \mathrm{diag}\{p_{k,n}\}$, $\mathbf{1}_{N_k}$ is a $N_k \times 1$ vector with all unitary entries, $\boldsymbol{C}_k$ stacks the residues vectors $\bar{\boldsymbol{R}}_{k,n}$ in its columns, and $\boldsymbol{D}_k = \boldsymbol{H}_{k,\infty}$. Using now (5), a global state-space realization is obtained for the entire macromodel as

$$\begin{cases} \dot{\tilde{\boldsymbol{x}}}(t) = \widetilde{\boldsymbol{A}}\tilde{\boldsymbol{x}}(t) + \widetilde{\boldsymbol{B}}\boldsymbol{u}(t) \\ \boldsymbol{y}(t) = \widetilde{\boldsymbol{C}}\tilde{\boldsymbol{x}}(t) + \widetilde{\boldsymbol{D}}\boldsymbol{u}(t) \end{cases} \tag{8}$$

where $\widetilde{\boldsymbol{A}}$ tiles in its diagonal the blocks $\boldsymbol{A}_k$. Moreover, if the port subsets Ω_k are ordered for increasing values of excitation index j_k, we have the general structure

$$\widetilde{\boldsymbol{A}} = \mathrm{blkdiag}\{\widetilde{\boldsymbol{A}}_i, i = 1, \ldots, P\}, \tag{9}$$

where

$$\widetilde{\boldsymbol{A}}_i = \mathrm{diag}\left\{(a_i)_q, q = 1, \ldots, N_i\right\} \tag{10}$$

collects all N_i poles for the ith column of $\boldsymbol{H}(s)$, and

$$\widetilde{\boldsymbol{B}} = \mathrm{blkdiag}\left\{\mathbf{1}_{N_i}, i = 1, \ldots, P\right\}. \tag{11}$$

The state-space realization (8) is characterized by complex matrices. However, an obvious coordinate change [24], [29] can be applied to recover a purely real realization

$$\begin{cases} \dot{\boldsymbol{x}}(t) = \boldsymbol{A}\boldsymbol{x}(t) + \boldsymbol{B}\boldsymbol{u}(t) \\ \boldsymbol{y}(t) = \boldsymbol{C}\boldsymbol{x}(t) + \boldsymbol{D}\boldsymbol{u}(t) \end{cases} \tag{12}$$

with $\boldsymbol{A} = \boldsymbol{P}^H\widetilde{\boldsymbol{A}}\boldsymbol{P}$, $\boldsymbol{B} = \boldsymbol{P}^H\widetilde{\boldsymbol{B}}$, $\boldsymbol{C} = \widetilde{\boldsymbol{C}}\boldsymbol{P}$, and $\boldsymbol{D} = \widetilde{\boldsymbol{D}}$ (superscript ^{H} denoting complex conjugate transpose). The unitary matrix $\boldsymbol{P}$ is block-diagonal with 1×1 unitary blocks corresponding to real poles and with 2×2 blocks

$$\frac{1}{\sqrt{2}}\begin{pmatrix} 1 & -j \\ 1 & j \end{pmatrix} \tag{13}$$

corresponding to complex conjugate pairs. This coordinate change induces the same block structure in $\boldsymbol{A}$, and preserves the sparsity pattern of $\widetilde{\boldsymbol{B}}$ in $\boldsymbol{B}$. This will be important in the following derivations.

B. Passivity Characterization via Hamiltonian Matrices

The real state-space realization of the macromodel in (12) is our starting point, with the associated transfer matrix being obtained directly from the state matrices as

$$\boldsymbol{H}(s) = \boldsymbol{D} + \boldsymbol{C}\left(s\boldsymbol{I} - \boldsymbol{A}\right)^{-1}\boldsymbol{B}. \tag{14}$$

We assume in the following that all poles, or equivalently the eigenvalues of $\boldsymbol{A}$, are strictly stable. Consequently, the transfer matrix $\boldsymbol{H}(s)$ is nonsingular for $\Re\{s\} \geq 0$. Since all state matrices are real, the passivity of $\boldsymbol{H}(s)$ can be checked only on the purely imaginary axis $s = j\omega$ via energy conditions that depend on the adopted representation. In the common case of scattering representations, passivity requires that all the singular values of the transfer matrix must be uniformly bounded by one at any frequency

$$\sigma_i \leq 1, \quad \forall \sigma_i \in \sigma\left(\boldsymbol{H}(j\omega)\right), \quad \forall \omega \tag{15}$$

whereas for the impedance, admittance, and hybrid cases the eigenvalues of the Hermitian part of the transfer matrix

$$\boldsymbol{G}(j\omega) = \frac{1}{2}\left(\boldsymbol{H}(j\omega) + \boldsymbol{H}^H(j\omega)\right) \tag{16}$$

must be nonnegative at any frequency

$$\lambda_i \geq 0, \quad \forall \lambda_i \in \lambda\left(\boldsymbol{G}(j\omega)\right), \quad \forall \omega. \tag{17}$$

Asymptotic (strict) passivity for large frequencies is insured when the direct coupling matrix $\boldsymbol{D}$ satisfies

$$\sigma_i < 1, \quad \forall \sigma_i \in \sigma(\boldsymbol{D}) \tag{18}$$

for the scattering case, and

$$\lambda_i > 0, \quad \forall \lambda_i \in \lambda(\boldsymbol{D}') \tag{19}$$

for the impedance, admittance, and hybrid cases, where $\boldsymbol{D}'$ and $\boldsymbol{D}''$ denote the symmetric and skew-symmetric parts of $\boldsymbol{D}$ according to

$$\boldsymbol{D} = \frac{1}{2}(\boldsymbol{D} + \boldsymbol{D}^T) + \frac{1}{2}(\boldsymbol{D} - \boldsymbol{D}^T) = \boldsymbol{D}' + \boldsymbol{D}''. \tag{20}$$

It is well known that a direct application of the above criteria to check and possibly enforce passivity may be cumbersome and misleading, since all frequencies must be considered. Fortunately, the Hamiltonian matrices associated to the state-space realization (12) provide an effective tool for deriving the passivity conditions in a purely algebraic form. Let us first recall the definitions of the Hamiltonian matrices for the scattering case,

$$\mathcal{M}_\gamma = \begin{pmatrix} \boldsymbol{A} - \boldsymbol{B}\boldsymbol{R}^{-1}\boldsymbol{D}^T\boldsymbol{C} & -\gamma\boldsymbol{B}\boldsymbol{R}^{-1}\boldsymbol{B}^T \\ \gamma\boldsymbol{C}^T\boldsymbol{S}^{-1}\boldsymbol{C} & -\boldsymbol{A}^T + \boldsymbol{C}^T\boldsymbol{D}\boldsymbol{R}^{-1}\boldsymbol{B}^T \end{pmatrix} \tag{21}$$

with $\boldsymbol{R} = (\boldsymbol{D}^T\boldsymbol{D} - \gamma^2\boldsymbol{I})$ and $\boldsymbol{S} = (\boldsymbol{D}\boldsymbol{D}^T - \gamma^2\boldsymbol{I})$, and for the hybrid cases

$$\mathcal{N}_\delta = \begin{pmatrix} \boldsymbol{A} + \boldsymbol{B}\boldsymbol{Q}^{-1}\boldsymbol{C} & \boldsymbol{B}\boldsymbol{Q}^{-1}\boldsymbol{B}^T \\ -\boldsymbol{C}^T\boldsymbol{Q}^{-1}\boldsymbol{C} & -\boldsymbol{A}^T - \boldsymbol{C}^T\boldsymbol{Q}^{-1}\boldsymbol{B}^T \end{pmatrix} \tag{22}$$

with $\boldsymbol{Q} = (2\delta\boldsymbol{I} - \boldsymbol{D} - \boldsymbol{D}^T)$. Both matrices depend on a scalar parameter, which is related to the spectrum of frequency-dependent singular values (γ, scattering case) or eigenvalues (δ, hybrid cases) of the transfer matrix $\boldsymbol{H}(s)$. We have the following two theorems [20] expressing this relation via the eigenspectrum of the Hamiltonian matrix.

***Theorem 1** (Scattering Representation):* Assume $\boldsymbol{A}$ has no imaginary eigenvalues, γ is not a singular value of $\boldsymbol{D}$, and $\omega_0 \in \mathbb{R}$. Then, $\gamma \in \sigma(\boldsymbol{H}(j\omega_0))$ if and only if $j\omega_0 \in \lambda(\mathcal{M}_\gamma)$.

***Theorem 2** (Impedance, Admittance, and Hybrid representations):* Assume $\boldsymbol{A}$ has no imaginary eigenvalues, δ is not an

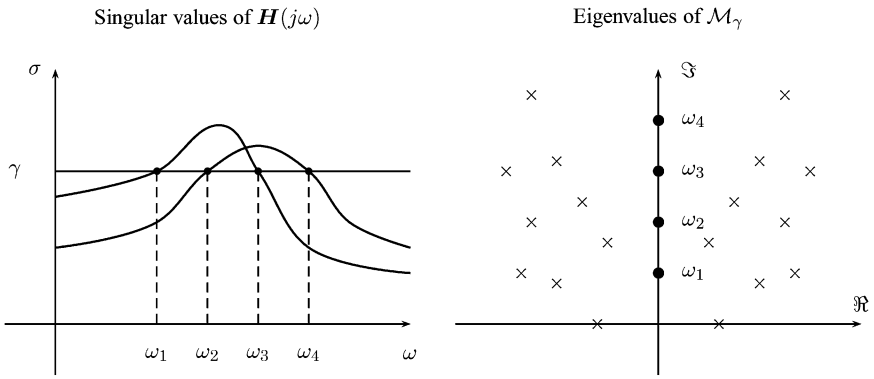

Fig. 1. Graphical illustration of Theorem 1, holding for the scattering case. The figure shows the one-to-one correspondence between the purely imaginary eigenvalues of the Hamiltonian matrix (right panel) and the frequencies where one of the singular values of the transfer matrix crosses or touches the threshold level γ (left panel).

eigenvalue of $\boldsymbol{D}'$, and $\omega_0 \in \mathbb{R}$. Then, $\delta \in \lambda(\boldsymbol{G}(j\omega_0))$ if and only if $j\omega_0 \in \lambda(\mathcal{N}_\delta)$.

Fig. 1 gives a schematic illustration of Theorem 1 for the scattering case. The scalar parameter γ acts as a threshold for the singular values of $\boldsymbol{H}(j\omega)$. Theorem 1 states that the purely imaginary eigenvalues of the Hamiltonian matrix pinpoint precisely the frequencies ω_i at which a singular value of $\boldsymbol{H}(j\omega)$ crosses or touches the threshold γ. Setting this threshold to the critical value for passivity ($\gamma = 1$ for the scattering case and $\delta = 0$ for the hybrid case), results in the algebraic passivity condition based on the Hamiltonian eigenspectrum, expressed by the following corollary.

***Corollary 1**:* Assume that $\boldsymbol{A}$ has no imaginary eigenvalues and that $\boldsymbol{D}$ satisfies the asymptotic passivity conditions (18) or (19). Then, the macromodel (12) is passive if the associated Hamiltonian matrix $\mathcal{M}_{\gamma=1}$ (scattering case) or $\mathcal{N}_{\delta=0}$ (hybrid case) has no purely imaginary eigenvalues.

The proof of all the above theorems (including some technical conditions for applicability) can be found in [20], [21], and [23]. We remark that in the very common case of multiple singular values exceeding the threshold in some frequency interval, as depicted in the left panel of Fig. 1, some ambiguity may arise in the determination of the actual frequency bands where passivity violations occur, since the only knowledge of the crossing points ω_i is not sufficient. However, the results in [21] and [23] show that a simple first-order perturbation analysis of the Hamiltonian eigenspectrum is sufficient for resolving this ambiguity.

C. Passivity Enforcement via Perturbation of Hamiltonian Matrices

Since imaginary eigenvalues of the Hamiltonian matrix indicate passivity violations, any passivity compensation scheme is aimed, either directly or indirectly, at eliminating them. Our approach, which follows from [23], is aimed at the direct perturbation of these eigenvalues in order to displace them from the imaginary axis. The full details of the algorithm are reported in [21] and [23]. We only recall here the main steps that are relevant for this work. These steps are summarized in Algorithm 1 and briefly commented as follows.

Algorithm 1 (passivity compensation): Compute a passive macromodel via iterative perturbation of imaginary eigenvalues of Hamiltonian matrix
Require: state-space matrices $\boldsymbol{A}$, $\boldsymbol{B}$, $\boldsymbol{C}$, $\boldsymbol{D}$

1: compute the set Λ of imaginary eigenvalues of $\mathcal{M}_{\gamma=1}$ (scattering) or $\mathcal{N}_{\delta=0}$ (hybrid)
2: compute the controllability Gramian $\boldsymbol{W}$
3: **while** $\Lambda \neq \emptyset$ **do**
4: determine the violation bandwidths from the imaginary eigenvalues in Λ [21]
5: set the desired perturbation $\boldsymbol{\delta\omega}$ of the imaginary eigenvalues (see [23])
6: solve (24) for $\boldsymbol{\Delta}$ with the constraint (25)
7: $\boldsymbol{C} \leftarrow \boldsymbol{C} + \boldsymbol{\Delta}$
8: compute the set Λ of imaginary eigenvalues of $\mathcal{M}_{\gamma=1}$ (scattering) or $\mathcal{N}_{\delta=0}$ (hybrid)
9: compute the controllability Gramian $\boldsymbol{W}$
10: **end while**

The main objective is the determination of a new macromodel obtained by suitable modifications of the state matrices. We assume asymptotic passivity and we retain the system poles. Therefore, the only modification that is strictly necessary applies to state matrix $\boldsymbol{C}$. The form of the new macromodel is thus

$$\begin{cases} \dot{\boldsymbol{x}}(t) = \boldsymbol{A}\boldsymbol{x}(t) + \boldsymbol{B}\boldsymbol{u}(t) \\ \boldsymbol{y}(t) = (\boldsymbol{C} + \boldsymbol{\Delta})\boldsymbol{x}(t) + \boldsymbol{D}\boldsymbol{u}(t) \end{cases}. \tag{23}$$

The key point of the compensation scheme is a first-order perturbation analysis [23], [30], which allows to relate the entries of the unknown perturbation matrix $\boldsymbol{\Delta}$ to the location of the perturbed imaginary eigenvalues of the Hamiltonian matrix associated to (23). The following linear expression is obtained:

$$\boldsymbol{Z}\mathrm{vec}(\boldsymbol{\Delta}) = \boldsymbol{\delta\omega} \tag{24}$$

where the operator $\mathrm{vec}(\cdot)$ stacks the columns of its argument, and the entries in vector $\boldsymbol{\delta\omega}$ are the perturbations of the imaginary eigenvalues. Matrix $\boldsymbol{Z}$ stems from the perturbation analysis [23]. The perturbed eigenvalues in (24) are selected *a priori* to move inwards into the violation bandwidths, as sketched in

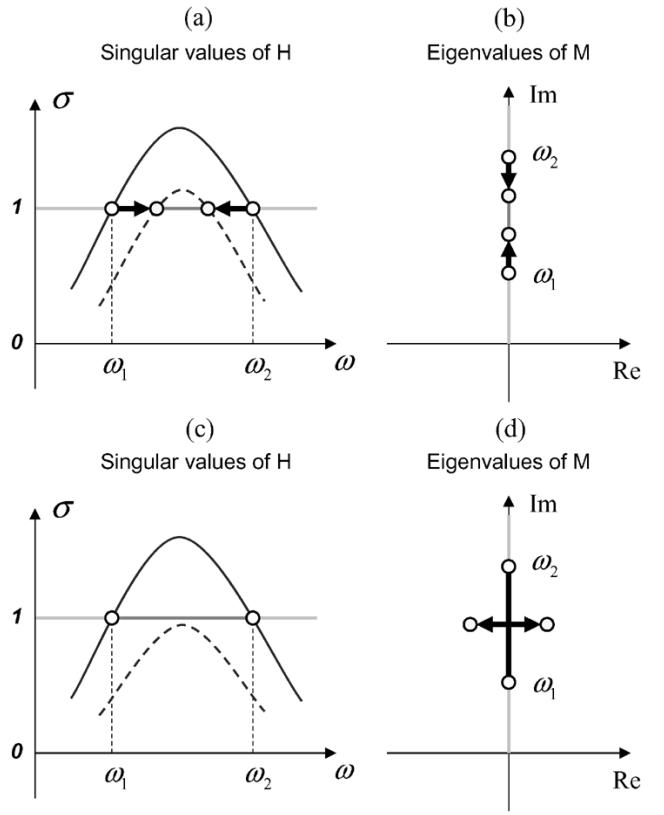

Fig. 2. Passivity compensation for scattering representations. Perturbation of eigenvalues of Hamiltonian matrix $\mathcal{M}$ (b) and its induced effect on the singular values of the macromodel (a). Iterative application leads to displacement of the eigenvalues off the imaginary axis (d) and consequently to passivity enforcement (c).

Fig. 2, and the underdetermined linear system (24) is solved by minimizing

$$\min \mathrm{Tr}\{\boldsymbol{\Delta W \Delta}^T\} \tag{25}$$

where $\mathrm{Tr}\{\cdot\}$ denotes the matrix trace and $\boldsymbol{W}$ is the controllability Gramian [31]. This condition is very important, since it guarantees the minimal impact on the macromodel accuracy [23]. Iterative solution of (24) and (25) leads to the elimination of all imaginary eigenvalues and, consequently, to passivity enforcement. Although the convergence properties of the algorithm are still under study, extensive experience has demonstrated that it is quite effective in the elimination of passivity violations that are not excessively large. Several examples of application of the scheme are available in [21], [23], and [32]. Other examples will be reported in Section VI.

D. Difficulties Arising With Large Macromodels

We outline here the main difficulties that arise in the application of the techniques of Section II for the passivity enforcement of large-sized macromodels. Three main points can be considered.

- The passivity enforcement scheme in Algorithm 1 is only able to process macromodels that are asymptotically passive for large frequencies. However, the response-splitting strategy (see Section II-A) that one is forced to employ for the derivation of a large-sized macromodel does not provide any control on asymptotic passivity. This problem is particularly relevant when the structure under consideration is nearly lossless up to the highest available frequency. Section III addresses this problem showing how $\boldsymbol{D}$ can be corrected to enforce asymptotic passivity. We also investigate in this section some issues related to the sensitivity of the macromodel with respect to this correction.
- The control over the accuracy in the iterative perturbation scheme in Algorithm 1 is provided by minimization of a matrix norm weighted by the controllability Gramian (25). This condition insures that no overtreatment occurs, and that macromodel accuracy is preserved through the iterations. However, the actual computation of the Gramian may require considerable computing resources, as well as its inclusion in the least-squares solution of (24). Section IV shows that the adopted structured state-space realization results in a block-diagonal controllability Gramian, which can be computed analytically. Therefore, the Gramian computation is not an issue for present formulation.
- The main tool for the formulation of the passivity compensation scheme is a first-order perturbation of the Hamiltonian eigenvalues. This requires computation of both imaginary eigenvalues and associated eigenvectors at each iteration. It is well known that the computational cost for this evaluation scales as the third power of the matrix size, which is $2N$ for the Hamiltonian matrix. Therefore, a large-sized macromodel requires prohibitive computing time. However, we show in Section V that the Hamiltonian matrix itself can be expressed as a low-rank perturbation of an almost-diagonal matrix. This allows an efficient application of a restarted Arnoldi scheme [26] with shift-and-invert spectral transformation for the computation of few selected eigenvalues close to a given point (shift) in the complex plane. Then, an iterative selection of multiple shifts similar to the well-known complex frequency hopping (CFH) algorithm [27] is used to extract all purely imaginary eigenvalues. The overall algorithm has a complexity that scales only linearly with the problem size, thus allowing its application for passivity compensation of large-sized macromodels at a moderate computational cost. A detailed description of the sparse eigenvalue solver, first introduced in [32], can be found in Section V.

III. Enforcing Asymptotic Passivity

We present here a simple scheme based on [16] for asymptotic passivity enforcement for both scattering [see (18)] and hybrid (19) representations. In addition, we give evidence of some critical issues related to the sensitivity of the macromodel accuracy with respect to asymptotic passivity enforcement.

We begin with the case of scattering representations. Let the singular value decomposition of $\boldsymbol{D}$ be expressed as

$$\boldsymbol{D} = \boldsymbol{U\Sigma V}^T \tag{26}$$

with left and right singular vectors stored in orthogonal matrices $\boldsymbol{U}$ and $\boldsymbol{V}$, and with Σ diagonal collecting the singular values σ_i in decreasing order. In case $\sigma_1 > 1$ so that passivity is violated, a simple correction is achieved by retaining the geometrical structure of $\boldsymbol{D}$, i.e., by preserving its singular vectors, and by thresholding its singular values to a maximum value less than one. We can define a new set of thresholded singular values

$$\widehat{\sigma}_i = \min\{\sigma_i, 1-\eta\}, \quad i = 1, \ldots, P, \quad 0 < \eta \leq 1. \tag{27}$$

Collecting the $\widehat{\sigma}_i$ in a diagonal matrix $\widehat{\boldsymbol{\Sigma}}$, we obtain a modified and strictly passive direct coupling matrix as

$$\widehat{\boldsymbol{D}} = \boldsymbol{U}\widehat{\boldsymbol{\Sigma}}\boldsymbol{V}^T. \tag{28}$$

Note that the positive parameter η determines a "safety margin" for asymptotic passivity. For η close to 0, small induced perturbations are obtained on the macromodel, which will be allowed to be characterized by an almost lossless behavior for large frequencies. Conversely, for η close to 1, larger perturbations are applied, with a more dissipative behavior of the macromodel for large frequencies.

For impedance, admittance, and hybrid representations, the same correction scheme can be applied. The eigendecomposition of the symmetric part $\boldsymbol{D}'$ of direct coupling matrix reads

$$\boldsymbol{D}' = \boldsymbol{\Psi}\boldsymbol{\Lambda}\boldsymbol{\Psi}^{-1} \tag{29}$$

with $\boldsymbol{\Lambda}$ collecting its purely real eigenvalues λ_i. If some of these eigenvalues are negative, a new asymptotically passive direct coupling matrix can be defined as

$$\widehat{\boldsymbol{D}} = \boldsymbol{\Psi}\widehat{\boldsymbol{\Lambda}}\boldsymbol{\Psi}^{-1} + \boldsymbol{D}'' \tag{30}$$

where the new thresholded eigenvalues are obtained as

$$\widehat{\lambda}_i = \max\{\lambda_i, \eta\lambda_{\max}\}, \quad i = 1, \ldots, P, \quad \eta > 0 \tag{31}$$

and $\lambda_{\max}$ is the largest magnitude among all λ_i. A similar correction strategy can be found in [16].

A perturbation of the direct coupling matrix $\bar{\boldsymbol{D}}$ as in (28) or (30) determines a translation of each transfer matrix entry by a constant amount throughout the frequency axis. Even for small perturbations, the resulting loss of accuracy of the macromodel can be quite significant. Therefore, after the redefinition of $\boldsymbol{D}$ into $\widehat{\boldsymbol{D}}$, a new fitting stage is required to adjust the macromodel parameters and to recover a good accuracy within the macromodel bandwidth. There are two possibilities. One is retain the macromodel poles and to recompute only the associated residues by constraining the values of the direct coupling constants. Alternatively, one can use one or more iterations of a pole relocation algorithm, such as vector fitting [8], in order to refine also the poles estimates. In all cases, the direct coupling constants must be kept fixed at their values obtained in (28) or (30). Both approaches lead generally to good results. However, when high-frequency poles are present in the macromodel, a sensitivity problem related to the high condition number of some matrices to be inverted may lead to a significant loss of accuracy and to larger passivity violations. In the following paragraphs, we investigate this issue via a simple but representative test case,

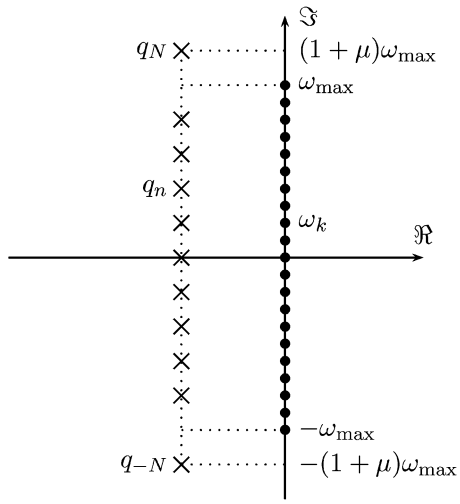

Fig. 3. Poles distribution (crosses) of a synthetic rational function employed for the sensitivity test. Dots indicate the frequency samples.

noting that for more complex situations encountered in practice the same conclusions will hold.

We consider a scalar one-port transfer function specified via a set of $2K+1$ linearly spaced frequency samples

$$\omega_k = \frac{k\omega_{\max}}{K}, \quad k = -K, \ldots, K \tag{32}$$

throughout the modeling bandwidth $[-\omega_{\max}, \omega_{\max}]$. Note that we include both positive and negative frequencies for simplicity in the presentation. The expression that we assume for the transfer function is

$$h(s) = h_\infty + \sum_{n=-N}^{N} \frac{r_n}{s - q_n} \tag{33}$$

with the $2N+1$ poles defined as

$$\begin{aligned} q_n &= -\alpha + \frac{jn\omega_{\max}}{N}, \quad n = -N+1, \ldots, N-1 \\ q_{\pm N} &= -\alpha \pm j\omega_{\max}(1+\mu). \end{aligned} \tag{34}$$

All poles share the same negative real part $-\alpha$ and have a linearly spaced imaginary part throughout the modeling bandwidth, except for the highest frequency ones $q_{\pm N}$, which are displaced by a relative amount μ outside $\omega_{\max}$. This setup (see Fig. 3 for a schematic illustration) is intended to illustrate the sensitivity of high-frequency poles to the perturbations induced by asymptotic passivity corrections.

The least squares system allowing to compute both residues and direct coupling term reads

$$(\boldsymbol{T} \quad \boldsymbol{1}_{2K+1}) \begin{pmatrix} \boldsymbol{r} \\ h_\infty \end{pmatrix} = \boldsymbol{h} \tag{35}$$

where $\boldsymbol{r}$ and $\boldsymbol{h}$ collect the unknown residues and the frequency samples $h(j\omega_k)$, respectively. The entries in matrix block $\boldsymbol{T}$ are

$$T_{kn} = \frac{1}{j\omega_k - q_n}, \quad k = -K, \ldots, K, \quad n = -N, \ldots, N. \tag{36}$$

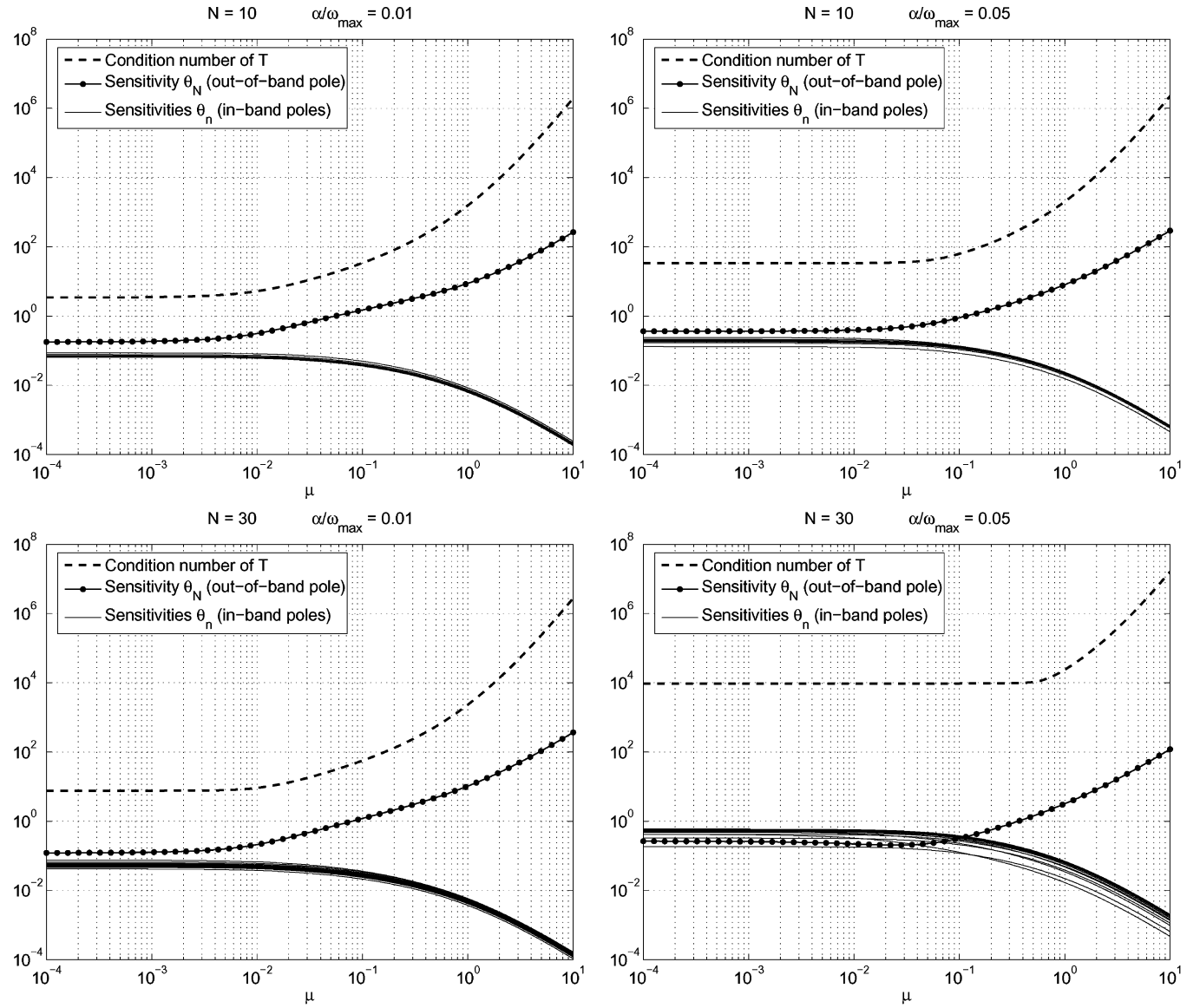

Fig. 4. Sensitivities of residues corresponding to in-band and out-of-band poles for various parameter configurations. Also, the condition number of the fitting matrix is reported in all panels.

Suppose now a solution has been obtained by solving (35) via standard least squares. A correction is applied to the direct coupling constant

$$\widehat{h}_\infty = h_\infty + \delta h_\infty \tag{37}$$

and a new least squares fit is formulated to recompute the residues with the prescribed value for $\widehat{h}_\infty$. The induced perturbation on the residues can be expressed as

$$\widehat{\boldsymbol{r}} = \boldsymbol{r} + \boldsymbol{\delta r} \tag{38}$$

and can be computed as the solution of

$$\boldsymbol{T}\boldsymbol{\delta r} = -\mathbf{1}_{2K+1}\delta h_\infty. \tag{39}$$

This solution, always in least-squares sense, reads

$$\boldsymbol{\delta r} = \left[-(\boldsymbol{T}^H\boldsymbol{T})^{-1}\boldsymbol{T}^H\mathbf{1}_{2K+1}\right]\delta h_\infty = \boldsymbol{\theta}\delta h_\infty. \tag{40}$$

The elements of vector $\boldsymbol{\theta}$ give the first-order perturbation terms on each residue induced by the correction in the direct coupling constant. These will be improperly denoted as sensitivities even though they represent absolute and not relative perturbations.

Fig. 4 reports the sensitivities θ_n of all residues for some different parameter configurations. The number of frequency samples is kept fixed with $K = 200$. The plots indicate that the sensitivities θ_n associated to the in-band poles are always less than one. This indicates good numerical stability of the associated residues under perturbation of the direct coupling constant. A different behavior is observed for the out-of-band poles. The associated sensitivities θ_N grow with the displacement of the poles outside the maximum frequency $\omega_{\max}$. Even for a small relative distance μ, the sensitivity becomes larger than one, depending on the number of poles and on their more or less resonant character. The plots also report the condition number of matrix $\boldsymbol{T}$, which results highly dependent on the parameter μ.

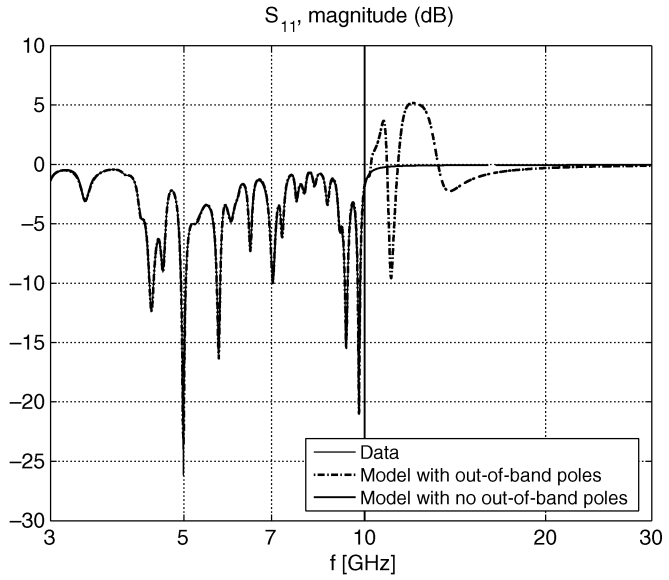

Fig. 5. Frequency response of two models (with and without out-of-band poles) obtained after asymptotic passivity correction, compared to the original data. Only the portion around the edge of the bandwidth (10 GHz) is shown.

These results confirm that occurrence of out-of-band poles (see [33] for a thorough discussion) should be carefully avoided in the generation of macromodels. When these poles appear, e.g., due to the poles relocation stages of vector fitting iterations, they should be either removed or displaced in order to avoid numerical difficulties.

Further evidence for the effects of out-of-band poles is presented in Fig. 5. The plot reports a comparison between original (scattering) data characterizing a two-port structure and two different models, differing only for the presence of out-of-band poles. A first model was obtained by vector fitting. Model was checked for asymptotic passivity, failing the test since the maximum singular value of the direct coupling matrix $\boldsymbol{D}$ was 1.024, slightly larger than one. The proposed correction scheme was applied by constraining the largest singular value of $\widehat{\boldsymbol{D}}$ to 0.9999, and the residues were recomputed via an additional least squares fit. This model was characterized by the presence of two pairs of complex conjugate poles located slightly outside the bandwidth of available frequency samples, in this case 10 GHz. For this reason, a second model was generated by first removing these poles and then by repeating the entire correction process. The magnitude responses of S_{11} for the two models are compared to the original data in Fig. 5. The plot clearly shows the sensitivity problem for the model including out-of-band poles, which exploits significant perturbations in the frequency region beyond 10 GHz. Instead, the model without out-of-band poles has a smooth and regular behavior throughout the frequency axis. Note also that the in-band behavior of both models is excellent. This example shows that a correction of asymptotic passivity may lead to dramatic passivity violations outside the modeling bandwidth when out-of-band poles are present. With these new induced violations, application of any passivity compensation scheme appears problematic. Therefore, any out-of-band poles should be removed before proceeding in the passivity enforcement. Note that in this case, it is not possible to circumvent this problem by extending the bandwidth of the model, as suggested in [33], since the frequency response of the original structure beyond the maximum available frequency is unknown.

IV. Sparse Evaluation of Controllability Gramian

As mentioned in Section II-C, a key step in the passivity compensation scheme is the evaluation of the controllability Gramian $\boldsymbol{W}$ associated to the state-space realization (12). It is well known that this step requires significant computational resources in case of large systems. Instead, we show that computation of the Gramian can be performed very efficiently due to the particular sparse structure adopted for the state matrices $\boldsymbol{A}$ and $\boldsymbol{B}$.

The controllability Gramian $\boldsymbol{W}$ is the solution of Lyapunov equation

$$\boldsymbol{A}\boldsymbol{W} + \boldsymbol{W}\boldsymbol{A}^T = -\boldsymbol{B}\boldsymbol{B}^T. \tag{41}$$

First, we note that $\boldsymbol{W}$ is related to the corresponding Gramian $\widetilde{\boldsymbol{W}}$ associated to the complex state-space realization (8) via

$$\boldsymbol{W} = \boldsymbol{P}^H \widetilde{\boldsymbol{W}} \boldsymbol{P} \tag{42}$$

where

$$\widetilde{\boldsymbol{A}}\widetilde{\boldsymbol{W}} + \widetilde{\boldsymbol{W}}\widetilde{\boldsymbol{A}}^H = -\widetilde{\boldsymbol{B}}\widetilde{\boldsymbol{B}}^H. \tag{43}$$

This second form is very convenient since $\widetilde{\boldsymbol{A}}$ is diagonal. Due to the block-diagonal form of $\widetilde{\boldsymbol{B}}$, we also have that the right-hand term is block-diagonal. More precisely

$$\widetilde{\boldsymbol{B}}\widetilde{\boldsymbol{B}}^H = \begin{pmatrix} \boldsymbol{U}_1 & \boldsymbol{0} & \dots & \boldsymbol{0} \\ \boldsymbol{0} & \boldsymbol{U}_2 & & \\ \vdots & & \ddots & \vdots \\ \boldsymbol{0} & & & \boldsymbol{U}_P \end{pmatrix} \tag{44}$$

with the ith block $\boldsymbol{U}_i$ having size $N_i \times N_i$ and all entries equal to one. Using the same induced block-partition for $\widetilde{\boldsymbol{W}}$ as

$$\widetilde{\boldsymbol{W}} = \begin{pmatrix} \widetilde{\boldsymbol{W}}_{11} & \widetilde{\boldsymbol{W}}_{12} & \dots & \widetilde{\boldsymbol{W}}_{1P} \\ \widetilde{\boldsymbol{W}}_{21} & \widetilde{\boldsymbol{W}}_{22} & & \\ \vdots & & \ddots & \vdots \\ \widetilde{\boldsymbol{W}}_{P1} & & & \widetilde{\boldsymbol{W}}_{PP} \end{pmatrix} \tag{45}$$

we can easily show that (43) decouples into the following set of smaller Lyapunov equations

$$\widetilde{\boldsymbol{A}}_i\widetilde{\boldsymbol{W}}_{ii} + \widetilde{\boldsymbol{W}}_{ii}\widetilde{\boldsymbol{A}}_i^H = -\boldsymbol{U}_i, \tag{46}$$

$$\widetilde{\boldsymbol{A}}_i\widetilde{\boldsymbol{W}}_{ij} + \widetilde{\boldsymbol{W}}_{ij}\widetilde{\boldsymbol{A}}_i^H = \boldsymbol{0}, \quad i \neq j. \tag{47}$$

The solution to each of these equations is available in analytical form due to the diagonal form of $\widetilde{\boldsymbol{A}}_i$ in (10). A straightforward derivation leads to an expression for the generic element (q, l) of each diagonal block $\widetilde{\boldsymbol{W}}_{ii}$

$$(\widetilde{\boldsymbol{W}}_{ii})_{q,l} = \frac{-(\boldsymbol{U}_i)_{q,l}}{(a_i)_q + (a_i)_l^*} = \frac{-1}{(a_i)_q + (a_i)_l^*}. \tag{48}$$

Note that under the working assumptions of simple and strictly stable poles $(a_i)_q$, the above solution is well defined since the

denominator cannot vanish. The same argument can be used to show that all elements in the off-diagonal blocks are vanishing, since (47) is nonsingular and homogeneous

$$\widetilde{\boldsymbol{W}}_{ij} = \boldsymbol{0}, \quad i \neq j. \tag{49}$$

In summary, the controllability Gramian is expressed in block-diagonal form as

$$\widetilde{\boldsymbol{W}} = \text{blkdiag}\{\widetilde{\boldsymbol{W}}_{ii}, i = 1, \ldots, P\}. \tag{50}$$

This structure is preserved also when the coordinate change in (42) is applied to recover the Gramian of the real realization (12). Note that this coordinate change requires negligible computing time since $\boldsymbol{P}$ is almost diagonal. As a result, steps 2 and 9 in Algorithm 1 can be performed at a computational cost which is negligible with respect to the other passivity compensation steps. The main bottleneck remains the evaluation of the imaginary eigenvalues of the Hamiltonian matrix. This issue is addressed next.

V. Evaluation of Imaginary Hamiltonian Eigenvalues

The discussion of Section II pointed that the computation of purely imaginary eigenvalues of Hamiltonian matrices plays a crucial role in checking and enforcing passivity of the associated macromodels. The simplest approach for this computation is to use a full eigenvalue solver in order to find the complete eigenspectrum of the Hamiltonian matrices, and to extract *a posteriori* the imaginary eigenvalues via thresholding of the real part. This approach is feasible only when the size of the problem is not too large, since the associated computational cost scales as the third power of the matrix size. Consequently, the overall cost for passivity check and compensation using Algorithm 1 would be excessive, since several eigenvalue computations are required per iteration [23].

We present in the following an algorithm for the selective computation of purely imaginary eigenvalues of Hamiltonian matrices associated to large and sparse macromodels. In fact, since the eigenvalues with a nonvanishing real part are of no interest, no computational effort should be spoiled to compute them. The basic numerical tool that we use is the well-known Arnoldi iteration [25], [26] with shift-and-invert spectral transformation, explicit restarts and deflation. This algorithm allows to find a small number of eigenvalues that are closest to a specific point ϑ in the complex plane. An iterative selection of multiple shifts located on the positive imaginary axis, similar to the CFH algorithm [27], is then used to focus on the eigenvalues that are lying on or very close to the imaginary axis. Note that although structure-preserving methods exploiting the symmetry of the Hamiltonian eigenspectrum are available [34], we employ here a nonstructured Arnoldi iteration for the sake of simplicity.

First, we recall few basic facts about Hamiltonian matrices. These are actually the enabling factors for all subsequent derivations. We start with the Shermann–Morrison–Woodbory identity, proposed in the following Lemma [35].

Lemma 1 (Shermann–Morrison–Woodbury Formula): Let $\mathcal{A} = \mathcal{E} + \mathcal{U}\mathcal{V}^T$. Then

$$\mathcal{A}^{-1} = \mathcal{E}^{-1} - \mathcal{E}^{-1}\mathcal{U}(\mathcal{I} + \mathcal{V}^T\mathcal{E}^{-1}\mathcal{U})^{-1}\mathcal{V}^T\mathcal{E}^{-1}. \tag{51}$$

This result allows to compute efficiently the inverse of a low-rank perturbation of a matrix $\mathcal{E}$, provided that $\mathcal{E}^{-1}$ is easy to compute and that the number of columns of $\mathcal{U}$ and $\mathcal{V}$ is small. Introduction of this Lemma is justified by the following decompositions of the Hamiltonian matrices (21) and (22), which can be derived by simple algebraic manipulations. In the scattering case we have

$$\mathcal{M}_\gamma = \begin{pmatrix} \boldsymbol{A} & \\ & -\boldsymbol{A}^T \end{pmatrix} + \begin{pmatrix} \boldsymbol{B} & \\ & -\boldsymbol{C}^T \end{pmatrix} \times \begin{pmatrix} -\boldsymbol{D} & \gamma\boldsymbol{I} \\ \gamma\boldsymbol{I} & -\boldsymbol{D}^T \end{pmatrix}^{-1} \begin{pmatrix} \boldsymbol{C} & \\ & \boldsymbol{B}^T \end{pmatrix} \tag{52}$$

whereas, for impedance, admittance, and hybrid representations

$$\mathcal{N}_\delta = \begin{pmatrix} \boldsymbol{A} & \\ & -\boldsymbol{A}^T \end{pmatrix} + \begin{pmatrix} \boldsymbol{B} \\ -\boldsymbol{C}^T \end{pmatrix} (2\delta\boldsymbol{I} - \boldsymbol{D} - \boldsymbol{D}^T)^{-1} (\boldsymbol{C} \quad \boldsymbol{B}^T). \tag{53}$$

Since we consider in this work only sparse state-space realizations with almost diagonal $\boldsymbol{A}$ (see Section II-A), the first block in (52) and (53) can be inverted analytically, and results in an almost diagonal inverse. Moreover, the inner matrices that need to be inverted in (52) and (53) have a small size ($2P$ and P, respectively) compared to the size of $\boldsymbol{A}$. As a consequence, application of Lemma 1 allows to compute quite efficiently the inverse of the Hamiltonian matrices. More generally, if we introduce a generic complex shift ϑ, a straightforward derivation leads to an expression for the so-called shifted inverse of both Hamiltonian matrices

$$(\mathcal{M}_\gamma - \vartheta\mathcal{I})^{-1} = \begin{pmatrix} \boldsymbol{A}_\vartheta & \\ & -\boldsymbol{A}_{-\vartheta}^T \end{pmatrix} - \begin{pmatrix} \boldsymbol{A}_\vartheta & \\ & -\boldsymbol{A}_{-\vartheta}^T \end{pmatrix} \begin{pmatrix} \boldsymbol{B} & \\ & -\boldsymbol{C}^T \end{pmatrix} \times \begin{pmatrix} -\boldsymbol{H}_\vartheta & \gamma\boldsymbol{I} \\ \gamma\boldsymbol{I} & -\boldsymbol{H}_{-\vartheta}^T \end{pmatrix}^{-1} \begin{pmatrix} \boldsymbol{C} & \\ & \boldsymbol{B}^T \end{pmatrix} \begin{pmatrix} \boldsymbol{A}_\vartheta & \\ & -\boldsymbol{A}_{-\vartheta}^T \end{pmatrix} \tag{54}$$

and

$$(\mathcal{N}_\delta - \vartheta\mathcal{I})^{-1} = \begin{pmatrix} \boldsymbol{A}_\vartheta & \\ & -\boldsymbol{A}_{-\vartheta}^T \end{pmatrix} - \begin{pmatrix} \boldsymbol{A}_\vartheta & \\ & -\boldsymbol{A}_{-\vartheta}^T \end{pmatrix} \begin{pmatrix} \boldsymbol{B} \\ -\boldsymbol{C}^T \end{pmatrix} \times \left(2\delta\boldsymbol{I} - \boldsymbol{H}_\vartheta - \boldsymbol{H}_{-\vartheta}^T\right)^{-1} (\boldsymbol{C} \quad \boldsymbol{B}^T) \begin{pmatrix} \boldsymbol{A}_\vartheta & \\ & -\boldsymbol{A}_{-\vartheta}^T \end{pmatrix} \tag{55}$$

where $\boldsymbol{A}_{\pm\vartheta} = (\boldsymbol{A} \pm \vartheta\boldsymbol{I})^{-1}$ and $\boldsymbol{H}_{\pm\vartheta} = \boldsymbol{D} - \boldsymbol{C}\boldsymbol{A}_{\pm\vartheta}\boldsymbol{B}$. The number of operations required by the above computations has a leading term which scales as $O(8N + 2M)$, where M is the total number of nonvanishing entries in $\boldsymbol{B}$ and $\boldsymbol{C}$. This cost is, therefore, linear in the number of macromodel states N.

The above results are now used for the determination of the Hamiltonian eigenvalues. Since the basic scheme is applicable with no difference both to scattering and hybrid representations, we use the generic notation $\mathcal{H}$ to denote the Hamiltonian matrix (52) or (53). The fast evaluation of the shifted Hamiltonian inverse via (54) or (55) allows a straightforward application of

the basic shifted Arnoldi process (see [26], [36] for an excellent review and a complete bibliographic database). This algorithm builds a d-dimensional orthogonal basis

$$\boldsymbol{V}_d = [\boldsymbol{v}_1, \ldots, \boldsymbol{v}_d] \tag{56}$$

of the Krylov subspace

$$\mathcal{K}^d\left((\mathcal{H} - \vartheta\mathcal{I})^{-1}, \boldsymbol{v}_1\right) = \operatorname{span}\left\{\boldsymbol{v}_1, (\mathcal{H} - \vartheta\mathcal{I})^{-1}\boldsymbol{v}_1, \ldots, (\mathcal{H} - \vartheta\mathcal{I})^{-d+1}\boldsymbol{v}_1\right\} \tag{57}$$

starting from an initial vector $\boldsymbol{v}_1$. This is performed by constructing one vector of the sequence (57) at the time and orthonormalizing it with respect to previous vectors, e.g., using a modified Gram–Schmidt procedure. During the iterations, also the Hessemberg matrix

$$\widetilde{\boldsymbol{H}}_d = \boldsymbol{V}_d^H(\mathcal{H} - \vartheta\mathcal{I})^{-1}\boldsymbol{V}_d \tag{58}$$

is constructed. This is a low-order Galerkin projection onto the Krylov subspace. It can be shown [36] that a few eigenvalues ξ_j (less than d) of $\widetilde{\boldsymbol{H}}_d$ provide good approximations $\widehat{\lambda}_j$ to some true eigenvalues λ_j of the original matrix $\mathcal{H}$ close to the shift ϑ

$$\widehat{\lambda}_j = \vartheta + \frac{1}{\xi_j} \simeq \lambda_j \tag{59}$$

An estimate of the corresponding eigenvectors $\widehat{\boldsymbol{z}}_j$ is easily derived, since these span the same Krylov subspace generated by vectors $\boldsymbol{v}_j$. It can be shown that

$$\widehat{\boldsymbol{z}}_j = \boldsymbol{V}_d\boldsymbol{u}_j \tag{60}$$

where $\boldsymbol{u}_j$ represent the eigenvectors of the projected matrix $\widetilde{\boldsymbol{H}}_d$.

For present application, the orthogonalization stage is the most demanding part of the basic Arnoldi scheme, requiring approximately $O(4Nd^2)$ operations. Therefore, it is desirable to use a small dimension d of the Krylov subspace in order to limit the computational cost. However, this choice might seriously impair convergence. Therefore, we use the scheme outlined in Algorithm 2, which employs explicit restarting and deflation [26], [37]. For the seek of clarity in the presentation, we focus on the restarting scheme first and we postpone the description of the deflation process, although they are intermixed in the various steps of Algorithm 2.

Algorithm 2 (Arnoldi iteration with explicit restarts and deflation): compute N_λ eigenvalues of matrix $\mathcal{H}$ close to a given shift ϑ
Require: a matrix $\mathcal{H}$, a shift ϑ.
Require: control parameters N_λ (number of desired eigenvalues), d (dimension of Krylov subspace), ε (tolerance)

1: $k = 1$
2: **while** $k \leq N_\lambda$ **do**
3: pick a random starting vector $\boldsymbol{v}_k \perp \boldsymbol{v}_j$, $j = 1, \ldots, k-1$, with $\|\boldsymbol{v}_k\| = 1$
4: **for** $j = k, \ldots, d-1$ **do**
5: $\boldsymbol{w} = (\mathcal{H} - \vartheta\mathcal{I})^{-1}\boldsymbol{v}_j$
6: **for** $i = 1, \ldots, j$ **do**
7: $h_{ij} = \boldsymbol{w}^H\boldsymbol{v}_i$
8: $\boldsymbol{w} \leftarrow \boldsymbol{w} - h_{ij}\boldsymbol{v}_i$
9: **end for**
10: $h_{j+1,j} = \|\boldsymbol{w}\|$
11: $\boldsymbol{v}_{j+1} = \boldsymbol{w}/h_{j+1,j}$
12: **end for**
13: compute the approximate eigenpairs (59)–(60) and pick the one $(\widehat{\lambda}_k, \widehat{\boldsymbol{z}}_k)$ with smallest residual norm (61)
14: orthonormalize the eigenvector against all previous vectors: $\boldsymbol{v}_k \leftarrow \widehat{\boldsymbol{z}}_k - \sum_{i=1}^{k-1}(\widehat{\boldsymbol{z}}_k^H\boldsymbol{v}_i)\boldsymbol{v}_i$, and $\boldsymbol{v}_k \leftarrow \boldsymbol{v}_k/\|\boldsymbol{v}_k\|$
15: **if** $\delta_k < \varepsilon$ **then**
16: $h_{ik} = \boldsymbol{v}_i^H\mathcal{H}\boldsymbol{v}_k$, $i = 1, \ldots, k$
17: $k \leftarrow k + 1$ {accept eigenpair and go to the next}
18: **else**
19: **go to** step 4 {restart the iterations}
20: **end if**
21: **end while**

The restarting scheme is best understood by setting $k = 1$, as in step 1. The first step is the selection of a random starting vector with unitary norm (step 3). Since $k = 1$ in the first pass of the while loop (step 2), there are no previous vectors $\boldsymbol{v}_j$ for the orthogonality enforcement in step 3. Steps 4–12 perform the standard Arnoldi iterations by constructing the orthogonal vectors $\boldsymbol{v}_j$ and the Hessemberg matrix $\widetilde{\boldsymbol{H}}_d = (h_{ij})$. The approximate eigenpairs $(\widehat{\lambda}_i, \widehat{\boldsymbol{z}}_i)$ are then computed via (59) and (60), and the one with least residual norm

$$\delta_i = \|\mathcal{H}\widehat{\boldsymbol{z}}_i - \widehat{\lambda}_i\widehat{\boldsymbol{z}}_i\| \tag{61}$$

is selected. This eigenpair is denoted in the following as $(\widehat{\lambda}_k, \widehat{\boldsymbol{z}}_k)$ in step 13. Two cases may apply at this point. If the residual norm is still larger than a prescribed accuracy ε, the eigenpair needs refinement. Therefore, a new starting vector $\boldsymbol{v}_k$ is defined from the eigenvector $\widehat{\boldsymbol{z}}_k$, and the Arnoldi iterations are restarted (step 19). This strategy is effective since this new starting vector is expected to have a large component in the dominant eigenspace that is being computed. Instead, if the residual norm is sufficiently accurate, the eigenpair $(\widehat{\lambda}_k, \widehat{\boldsymbol{z}}_k)$ is accepted (step 17) and deflation is performed to achieve convergence of other eigenpairs.

Deflation is performed by the loop in step 2. The main idea is to lock the already converged vectors $\boldsymbol{v}_j$ for $j = 1, \ldots, k-1$ while computing the kth eigenpair. New Krylov vectors are added to this existing set, by completing the space via $(d-k)$ Arnoldi steps (step 4). This procedure leads to "modified" Krylov subspace

$$\operatorname{span}\left\{\boldsymbol{v}_1, \ldots, \boldsymbol{v}_{k-1}, \boldsymbol{v}_k, (\mathcal{H} - \vartheta\mathcal{I})^{-1}\boldsymbol{v}_k, \ldots, (\mathcal{H} - \vartheta\mathcal{I})^{-d+k}\boldsymbol{v}_k\right\} \tag{62}$$

where only the last $(d-k)$ components are added and orthogonalized with respect to all existing vectors (steps 5–9). The initial starting vector $\boldsymbol{v}_k$ in step 3 is chosen to be orthogonal to the locked vectors, in order to guarantee convergence of different

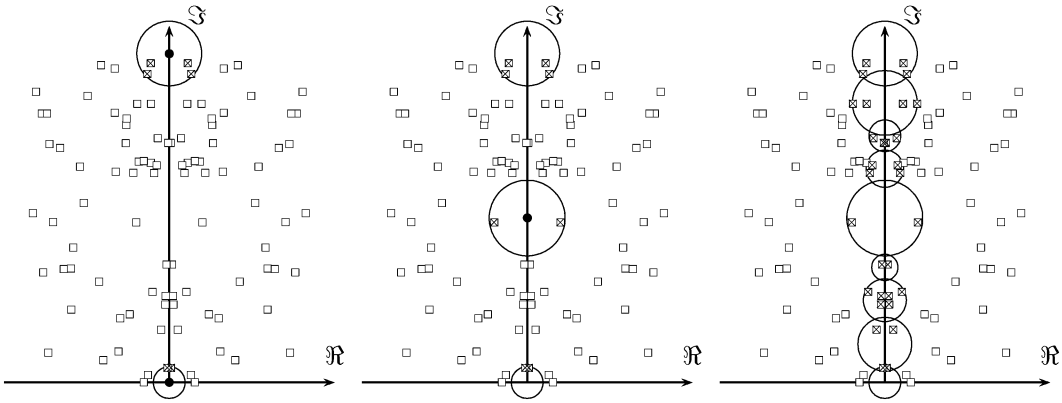

Fig. 6. Multishift iterations. Left: placement of two shifts (dots) at the edges of the frequency band. Middle: first bisection iteration. Right: termination condition with the convergence circles covering all frequency band. In all panels, the squares denote all Hamiltonian eigenvalues, and the crosses denote converging eigenvalues from the single-shift iterations.

eigenvalues. We remark that in the actual implementation of Algorithm 2, we test convergence of multiple eigenpairs instead of only one (steps 13–15) for each deflation step. Therefore, the number of passes in the main deflation loop (step 2) may be significantly less than the number N_λ of desired eigenpairs.

It is well known [26] that the closer is an eigenvalue to the shift, the faster is its convergence rate. However, it is not guaranteed (although very likely) that the N_λ eigenvalues that are returned by Algorithm 2 are really the closest to the shift. This condition, however, is essential for the subsequent derivations, which require for a given shift ϑ the accurate identification of all eigenvalues within a circular region

$$\Theta(\vartheta,\rho)=\{s:|s-\vartheta|\leq\rho\} \tag{63}$$

of the complex plane. The radius ρ is of course both problem- and shift-dependent, and must be determined together with the eigenvalues. We deal with this issue by defining an initial radius as

$$\rho=\max_k|\widehat{\lambda}_k-\vartheta| \tag{64}$$

from the set of converged eigenvalues after $n_\lambda<N_\lambda$ deflation steps. Then, all eigenpairs computed at step 13 in subsequent deflation passes are tested not only for convergence but also for their inclusion in $\Theta(\vartheta,\rho)$. If some eigenvalues appear within the circle without sufficient accuracy, they are refined until convergence is achieved.

Algorithm 2 with the optimizations discussed above leads to all eigenvalues of the Hamiltonian matrix within a circle $\Theta(\vartheta,\rho)$. We denote this scheme as *single-shift iterations*. The number of converging eigenvalues as well as the radius ρ depends on the entire eigenspectrum of $\mathcal{H}$ and on the location of the shift ϑ. In order to compute the complete set of purely imaginary eigenvalues of $\mathcal{H}$, we apply a bisection scheme, which we call *multishift iterations*, similar to the well-known CFH algorithm of [12], [27]. We only give an outline here since the CFH algorithm is well documented in the literature.

An illustrative description of the multishift scheme can be found in Fig. 6. First, an estimate of the largest magnitude $|\lambda|_{\max}$ among all Hamiltonian eigenvalues is obtained by applying Algorithm 2 (actually, a simplified version without deflation is sufficient) to matrix $\mathcal{H}$ instead of its shifted inverse [26]. Then, two single-shift iterations are performed by placing one shift at the origin of the complex plane, and the other at $j|\lambda|_{\max}$. The results are depicted in the left panel of Fig. 6, where converging eigenvalues and convergence circles are highlighted. Then, a bisection process is started by placing iteratively new shifts on the imaginary axis, close to the center of the frequency bands that are not covered by circles. Algorithm 2 is then applied (middle panel of Fig. 6) for each shift of the binary tree and the process is iterated. The algorithm stops when the entire portion of the imaginary axis $\omega\in[0,|\lambda|_{\max}]$ is covered by a collection of circles (right panel in Fig. 6).

The multishift iterations lead to a collection of estimates $\widehat{\lambda}_k$ for the eigenvalues that are close to the imaginary axis, as the set of all converging eigenvalues from all employed shifts. Since only the purely imaginary eigenvalues are of interest, these must be extracted by a suitable thresholding criterion. The simplest approach is to set a stringent threshold ϵ for the real part, and to retain only those eigenvalues such that

$$\left|\Re\{\widehat{\lambda}_k\}\right|<\epsilon|\lambda|_{\max}. \tag{65}$$

The choice of this threshold may be critical, since (65) does not take into account the accuracy of the obtained eigenvalue estimates. However, an accuracy measure is actually available via the residual norms in (61). These can be used to obtain, via a first-order perturbation analysis, the following estimate:

$$\Delta\lambda_k=|\widehat{\lambda}_k-\lambda_k|\sim\frac{\max\{\delta_k,\widetilde{\delta}_k\}}{\left|\widetilde{\boldsymbol{z}}_k^T\widehat{\boldsymbol{z}}_k\right|} \tag{66}$$

where λ_k is the exact eigenvalue, $\widetilde{\boldsymbol{z}}_k$ is the eigenvector of $\mathcal{H}^T$ corresponding to the same eigenvalue $\widehat{\lambda}_k$, and $\widetilde{\delta}_k$ is its associated residual norm. The (left) eigenvectors $\widetilde{\boldsymbol{z}}_k$ can be computed by applying Algorithm 2 to matrix $(\mathcal{H}^T-\widehat{\lambda}_k\mathcal{I})^{-1}$, i.e., the inverse of the transposed Hamiltonian matrix shifted in the computed eigenvalues. Since it is expected that $\widehat{\lambda}_k$ is very close to a true eigenvalue, the convergence rate is very fast and few iterations are sufficient. The quantity $\Delta\lambda_k$ can be used as an indication of the accuracy of the computed eigenvalues $\widehat{\lambda}_k$. Note that the factor at the denominator in (66), which is related to the angle between left and right eigenvectors, determines an amplification factor for the residual norms. To summarize, a better

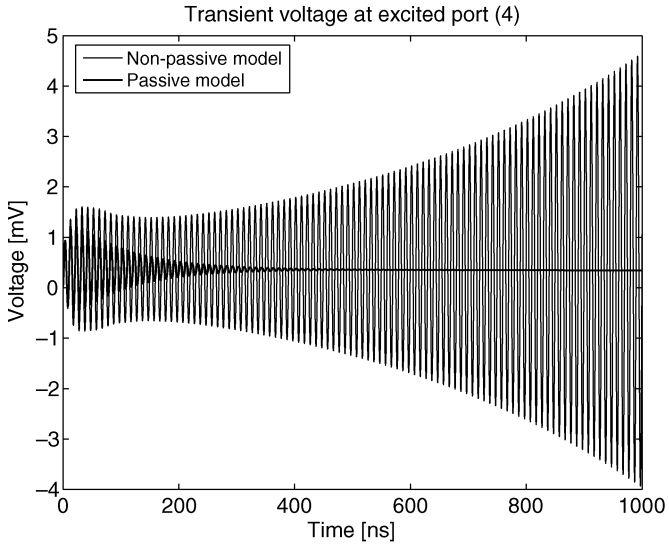

Fig. 7. Transient SPICE simulation of case IV macromodel before and after passivity enforcement. The same termination (a 143-mΩ resistor in series with a parallel connection of a 17.4-kΩ resistor and a 2.13-nF capacitor) is used for all ports. This load induces a pair of unstable poles $p = (0.0018 \pm j0.628)$ Grad/s in the nonpassive macromodel. A current source $i_s(t) = I_0 e^{-\alpha t}\sin(2\pi f_0 t)$ with $I_0 = 1$ mA, $\alpha = 0.01$ ns^{-1}, and $f_0 = 0.1$ GHz injects energy at port 4, exciting the unstable pole of the nonpassive model. As expected, the passive model remains stable.

(additional) criterion for the discrimination of the purely imaginary eigenvalues could be defined by comparing the real part with the accuracy

$$\left|\Re\{\widehat{\lambda}_k\}\right| < c\Delta\lambda_k \tag{67}$$

where $c > 1$ is a suitable constant. If this condition is not satisfied, the eigenvalue is flagged as non purely imaginary and rejected. The actual test that was implemented is the simpler (65), since we have never experienced any eigenvalue misidentification during the many performed validations. However, it is conceivable that particular cases with a strongly ill-conditioned eigenspectrum may require more advanced testing conditions, such as (67).

In summary, all steps of both single-shift and multishift iterations require a computational cost which scales linearly with the number of macromodel states N. It is clear that since several nested iterations are required, the leading term in the operation count is $O(CN)$, where the constant C is problem-dependent and possibly large. However, we show in Section VI that the gain in efficiency arising from application of the proposed algorithm with respect to a standard full eigensolver can be quite significant.

VI. Numerical Results

Numerical results will be presented for five different macromodels of various size, listed in Table I. All models were obtained by various implementations of the well-known vector fitting algorithm [8], applied to frequency-dependent scattering matrices. In particular, cases I and II are high-speed packaging structures (courtesy of Sigrity, Inc.). These two cases were already analyzed in [32]. Case III is also a model of a six-port interconnected system including two power/ground conductors

TABLE I
Specification of Five Nonpassive Macromodels. The Largest Singular Values for Each Model and for the Corresponding Raw Data are Reported in the Last Two Columns, Respectively

Model	Poles N	Ports P	$\sigma_{\max}$ (model)	$\sigma_{\max}$ (raw data)
Case I	820	10	1.003	$\lesssim 1$
Case II	1488	12	1.004	$\lesssim 1$
Case III	450	6	1.002	1.0003
Case IV	600	20	1.009	0.9996
Case V	1000	20	1.002	0.9996

(ports 1 and 2), and two signal conductors, terminated by ports 3–6. The raw data for this structure was obtained using a full-wave solver based on finite integration in time domain (CST Microwave Studio), and fast Fourier transform (FFT) was used to extract the frequency-dependent scattering matrix. Cases IV and V are two macromodels of a 20-port via field under a land grid array (LGA) connector, generated from the same frequency-dependent scattering matrix (courtesy of IBM), computed via a full-wave solver based on finite elements (Ansoft HFSS). These two models differ only for the number of poles that were used in the rational approximation. Some selected responses for each test case are depicted in Fig. 9.

Most of the model passivity violations (fourth column in Table I) are generated in the first model fit to the raw data, although in some cases (case III) also the raw data is nonpassive. The main reason for this loss of passivity is due to the almost lossless character of most interconnect structures, especially at low frequencies. It is obvious that good quality data (i.e., passive or almost passive) helps in the derivation of a good model, since the model passivity violations will be mostly due to the fitting error. In fact, in all cases the model passivity violations are quite limited, since the maximum singular value $\sigma_{\max}$ exceeds the threshold $\gamma = 1$ by a small amount. Nonetheless, it is guaranteed [14] that there exists a passive termination network that drives the model to instability, as demonstrated in Fig. 7 for Case IV. Therefore, passivity enforcement is mandatory.

We begin by showing the advantages of the scheme proposed in Section IV for the evaluation of the controllability Gramian $\boldsymbol{W}$. The Gramian was computed for each of the five test cases using three different algorithms. The first scheme neglected the sparse structure of the state-space matrices $\boldsymbol{A}$ and $\boldsymbol{B}$, and the standard Schur decomposition approach [38] for the solution of the Lyapunov equation (41) was used. The second scheme used a dedicated Schur decomposition exploiting the sparse (almost diagonal) structure of $\boldsymbol{A}$. However, no hypotheses on the sparsity of $\boldsymbol{B}$ were applied, leading to a nonsparse representation of the Gramian $\boldsymbol{W}$. Finally, the third scheme is the one proposed in Section IV. The CPU time required by the three schemes is reported in Table II. The algorithms were run within Matlab environment on a Pentium IV-based notebook running at 2.2 GHz. The results show clearly that the proposed scheme gives the best performance, whereas other implementations that do not take advantage of the structured state-space realization are quite inefficient. The speedup factor for these tests ranges from 44 to 289 for the largest model (Case II).

We turn now to the application of the complete passivity enforcement scheme (Algorithm 1), in order to quantify the improvements that can be achieved using the sparse eigenvalue

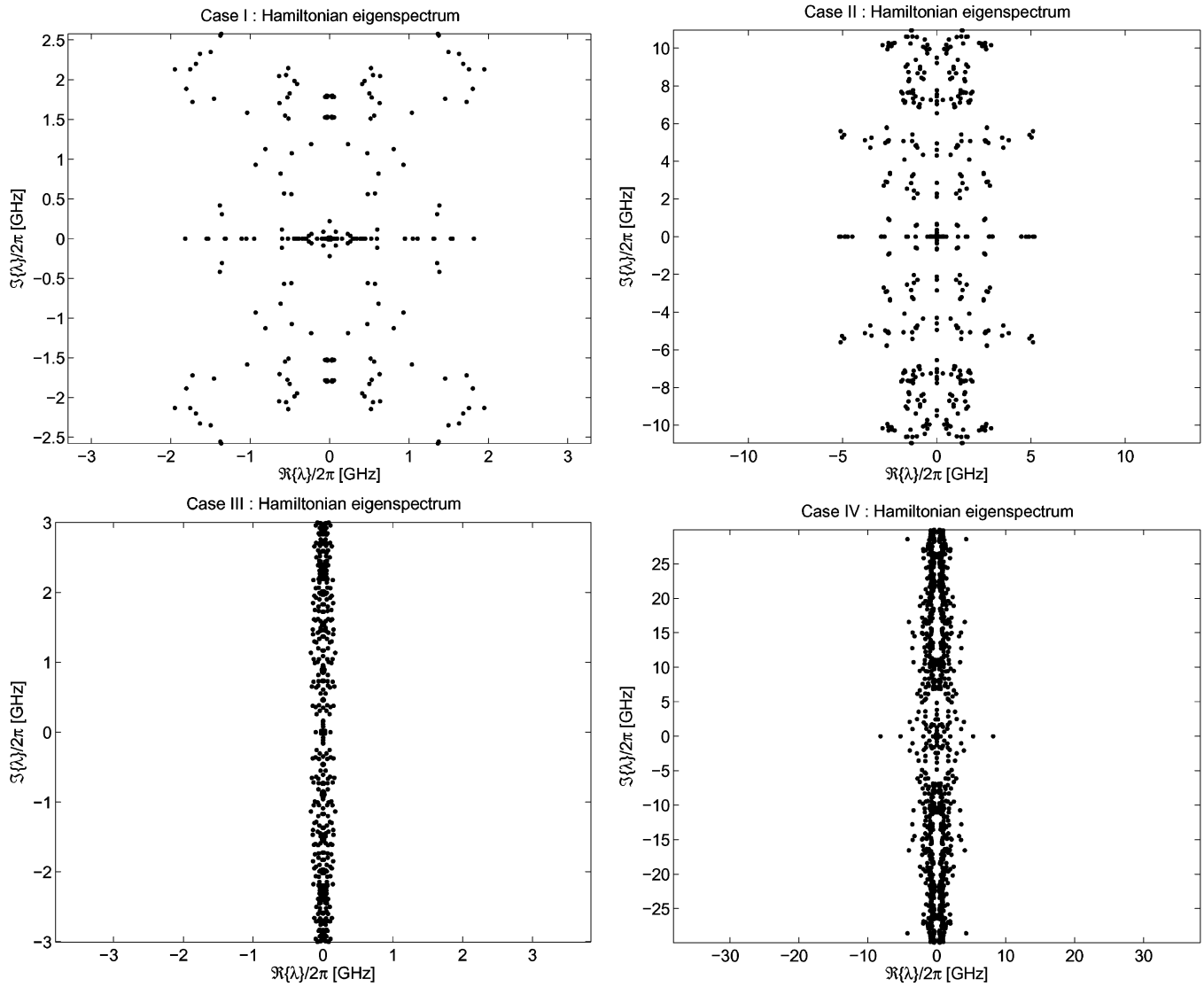

Fig. 8. Full spectrum of Hamiltonian eigenvalues for test cases I-IV. The total number of eigenvalues is 1640 (case I), 2976 (case II), 900 (case III), and 1200 (case IV).

TABLE II
CPU TIME IN SECONDS REQUIRED BY THE EVALUATION OF THE CONTROLLABILITY GRAMIAN. ALL COMPUTATIONS WERE PERFORMED WITH A PENTIUM IV (2.2 GHz)-BASED NOTEBOOK

Model	Full $\boldsymbol{A}$ and $\boldsymbol{B}$	Sparse $\boldsymbol{A}$, full $\boldsymbol{B}$	Sparse $\boldsymbol{A}$ and $\boldsymbol{B}$
Case I	152	15	1.7
Case II	983	62	3.4
Case III	30	4.2	0.68
Case IV	71	7.2	1.3
Case V	323	19	1.9

TABLE III
RESULTS OF PASSIVITY COMPENSATION SCHEMES APPLIED TO THE SAME TEST CASES OF TABLE II. MODELS I AND II WERE ANALYZED USING A PC WITH A 1.8-GHz PENTIUM IV CPU, WHILE FOR THE OTHER MODELS A FASTER 3-GHz PC WAS USED

Model	Iterations	CPU (full)	CPU (sparse)	Speedup
Case I	9	119 min	9.1 min	13
Case II	13	21 hrs	15 min	84
Case III	13	16 min	6.6 min	2.4
Case IV	20	36 min	14 min	2.6
Case V	13	77 min	35 min	2.2

solver proposed in Section V. The results are summarized in Table III. The second column of the table reports the number of iterations required by the compensation algorithm to reach passivity (this iteration count is independent on the adopted eigenvalue solver for the Hamiltonian matrix). The CPU time required for the passivity compensation run using either a standard eigensolver or the proposed optimized eigensolver are also reported in Table III (see the caption for hardware details). These results show that in all cases, the proposed sparse solver leads to a speedup in CPU time with respect to a standard full solver. However, looking at the particular speedup factors that were achieved, one can easily subdivide the models into two different classes. Cases I and II show a significant gain, ranging between one and two orders of magnitude. The other cases show instead a moderate advantage, with a speedup factor ranging between two and three. This difference is easily understood from the distribution of the Hamiltonian eigenvalues in the complex plane. Fig. 8 shows the complete Hamiltonian eigenspectrum for cases I-IV (case V being very similar to case IV). In all panels, identical

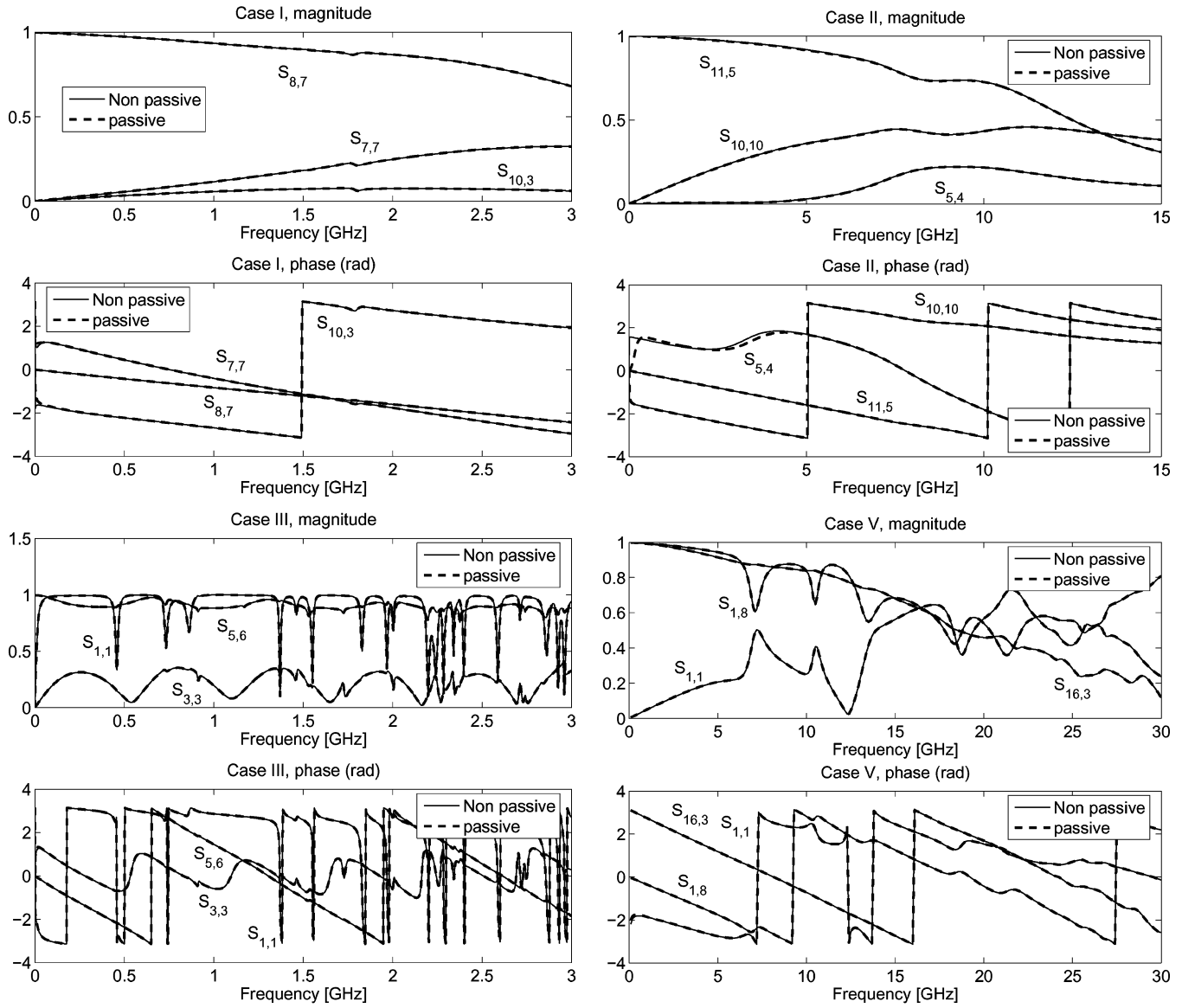

Fig. 9. Comparison of models before and after passivity compensation. For each case, the responses characterized by the largest deviations between nonpassive and passive models are reported.

scales for the real and the imaginary part have been chosen. This figure highlights the different nature of cases I and II, reported in the top panels, and cases III, IV, reported in the bottom panels. The former are characterized by a Hamiltonian eigenspectrum that is well separated from the imaginary axis, with a real part that is comparable to the imaginary part. In this case, a small number of complex shifts is sufficient to cover completely the relevant portion of the imaginary axis. In other words, the multishift iterations require few bisection steps. The latter models, instead, have a spectrum of eigenvalues that is very close to the imaginary axis. Consequently, a large number of small circles is needed to cover uniformly the imaginary axis and to terminate the multishift bisection process. The actual number of required shifts and bisection levels required by the computation of the imaginary eigenvalues for each of the test models are reported in Table IV. Since the CPU time is roughly proportional to the number of shifts and to the size of the Hamiltonian matrix, the moderate speedup factor for some of the models is easily understood. Note also that the number of imaginary eigenvalues has a negligible influence on the CPU time.

TABLE IV
COMPUTATION OF IMAGINARY EIGENVALUES. FOR EACH MODEL, THE NUMBER OF SHIFTS, THE BISECTION LEVEL, AND THE NUMBER OF IMAGINARY EIGENVALUES OF THE HAMILTONIAN MATRIX ARE REPORTED. THE LAST COLUMN REPORTS THE MAXIMUM RESIDUAL NORM (61) AMONG ALL COMPUTED EIGENVALUES

Model	Shifts	Bisections	Eigenvalues	Max Residual
Case I	19	4	1	1.7×10^{-14}
Case II	11	5	24	3.4×10^{-15}
Case III	57	7	14	2.1×10^{-14}
Case IV	37	6	7	2.2×10^{-14}
Case V	46	6	6	2.2×10^{-14}

We complete the presentation by comparing in Fig. 9 a few representative scattering responses of the passive models to the corresponding ones of the nonpassive models before applying the compensation scheme. For each case, the three responses

characterized by the largest modifications induced from the passivity compensation algorithm are depicted in magnitude and phase. The results reported in all panels show that, thanks to the accuracy constraint represented by (25), the deviation between the two models is hardly visible. This confirms that the passivity compensation is performed without compromising the accuracy, and that no overtreatment occurs.

VII. Conclusion

We have discussed several issues arising when enforcing passivity of macromodels characterized by a large number of poles and/or ports. In such cases, the main difficulties come from the excessive computational resources, both in terms of storage and CPU time, required by standard passivity compensation algorithms. Therefore, we adopted here a particular structured state-space form for the macromodels. This form allowed us to reformulate the critical steps of a recently developed passivity enforcement algorithm based on the spectral perturbation of Hamiltonian matrices. On one hand, this new formulation allows to compute efficiently the controllability Gramian, which is required to control the macromodel accuracy during the passivity compensation. On the other hand, it allows an efficient implementation of an iterative multishift restarted Arnoldi scheme for the selective evaluation of the purely imaginary eigenvalues of the Hamiltonian matrix. These eigenvalues are indeed the key parameters upon which the passivity enforcement is based. Finally, the preexisting restriction of asymptotic passivity at high frequencies is also released in this work, due to a specific correction strategy for the direct coupling matrix of the macromodel. As a result, the spectral perturbation approach for the Hamiltonian matrices has been extended and is now also applicable to large macromodels within a reasonable CPU time. The numerical results reported in this paper for a few cases of high-speed interconnects show indeed a significant increase in efficiency with respect to previous formulations.

Acknowledgment

The authors would like to thank J. Zheng (Sigrity, Inc.) for providing the test cases I and II, and to L. Shan and A. Deutsch (IBM) for providing the data for test cases IV and V.

References

[1] W. Beyene and J. Schutt-Ainé, "Accurate frequency-domain modeling and efficient circuit simulation of high-speed packaging interconnects," *IEEE Trans. Microw. Theory Tech.*, vol. 45, no. 10, pp. 1941–1947, Oct. 1997.

[2] K. L. Choi and M. Swaminathan, "Development of model libraries for embedded passives using network synthesis," *IEEE Trans. Circuits Syst. II, Analog Digit. Signal Process.*, vol. 47, no. 4, pp. 249–260, Apr. 2000.

[3] W. Do Couto Boaventura, A. Semlyen, M. Reza Iravani, and A. Lopes, "Sparse network equivalent based on time-domain fitting," *IEEE Trans. Power Del.*, vol. 17, no. 1, pp. 182–189, Jan. 2002.

[4] M. Elzinga, K. Virga, L. Zhao, and J. L. Prince, "Pole-residue formulation for transient simulation of high-frequency interconnects using householder LS curve-fitting techniques," *IEEE Trans. Compon. Packag. Manuf. Technol.*, vol. 23, no. 2, pp. 142–147, May. 2000.

[5] M. Elzinga, K. Virga, and J. L. Prince, "Improve global rational approximation macromodeling algorithm for networks characterized by frequency-sampled data," *IEEE Trans. Microw. Theory Tech.*, vol. 48, no. 9, pp. 1461–1467, Sep. 2000.

[6] S. Grivet-Talocia, F. Canavero, I. Maio, and I. Stievano, "Reduced-order macromodeling of complex multiport interconnects," in *URSI General Assembly*, Maastricht, Belgium, Aug. 19–23, 2002. BD.O.1 (1-4).

[7] S. Grivet-Talocia, "Package macromodeling via time-domain vector fitting," *IEEE Microw. Wireless Compon. Lett.*, vol. 13, no. 11, pp. 472–474, Nov. 2003.

[8] B. Gustavsen and A. Semlyen, "Rational approximation of frequency responses by vector fitting," *IEEE Trans. Power Del.*, vol. 14, no. 3, pp. 1052–1061, Jul. 1999.

[9] S. Grivet-Talocia, "Passive time-domain macromodeling of large complex interconnects," in *Proc. ACES04, 20th Annu. Rev. Progress in Applied Computational Electromagnetics*, Syracuse, NY, Apr. 19–23, 2004.

[10] S. Grivet-Talocia, F. G. Canavero, I. S. Stievano, and I. A. Maio, "Circuit extraction via time-domain vector fitting," in *Proc. IEEE Symp. EMC*, Santa Clara, CA, Aug. 9–13, 2004, pp. 1005–1010.

[11] M. Celik, L. Pileggi, and A. Obadasioglu, *IC Interconnect Analysis*. Norwell, MA: Kluwer, 2002.

[12] M. Nakhla and R. Achar, "Simulation of high-speed interconnects," *Proc. IEEE*, vol. 89, no. 5, pp. 693–728, May 2001.

[13] V. Belevitch, *Classical Network Theory*. San Francisco, CA: Holden-Day, 1968.

[14] K. Zhou, J. C. Doyle, and K. Glover, *Robust and Optimal Control*. Englewood Cliffs, NJ: Prentice-Hall, 1996.

[15] J. Morsey and A. C. Cangellaris, "PRIME: passive realization of interconnects models from measures data," in *Proc. IEEE 10th Topical Meeting on Electr. Perf. of Electron. Packag.*, 2001, pp. 47–50.

[16] B. Gustavsen and A. Semlyen, "Enforcing passivity for admittance matrices approximated by rational functions," *IEEE Trans. Power Syst.*, vol. 16, no. 1, pp. 97–104, Feb. 2001.

[17] C. P. Coelho, J. Phillips, and L. M. Silveira, "A convex programming approach for generating guaranteed passive approximations to tabulated frequency-data," *IEEE Trans. Comput.-Aided Des. Integr. Circuits Syst.*, vol. 23, no. 2, pp. 293–301, Feb. 2004.

[18] S. Boyd, L. El Ghaoui, E. Feron, and V. Balakrishnan, *Linear Matrix Inequalities in System and Control Theory, SIAM Studies in Applied Mathematics*. Philadelphia, PA: SIAM, 1994.

[19] H. Chen and J. Fang, "Enforcing bounded realness of S parameter through trace parameterization," in *Proc. 12th IEEE Topical Meeting on Electrical Performance of Electronic Packaging*, Princeton, NJ, Oct. 27–29, 2003, pp. 291–294.

[20] S. Boyd, V. Balakrishnan, and P. Kabamba, "A bisection method for computing the H_∞ norm of a transfer matrix and related problems," *Math. Control Signals Syst.*, vol. 2, pp. 207–219, 1989.

[21] S. Grivet-Talocia, "Enforcing passivity of macromodels via spectral perturbation of Hamiltonian matrices," in *Proc. 7th IEEE Workshop on Signal Propagation on Interconnects*, Siena, Italy, May 11–14, 2003, pp. 33–36.

[22] D. Saraswat, R. Achar, and M. Nakhla, "Enforcing passivity for rational function based macromodels of tabulated data," in *Proc. 12th IEEE Topical Meeting on Electrical Performance of Electronic Packaging*, Princeton, NJ, Oct. 27–29, 2003, pp. 295–298.

[23] S. Grivet-Talocia, "Passivity enforcement via perturbation of Hamiltonian matrices," *IEEE Trans. Circuits Syst. I, Fundam. Theory Appl.*, vol. 51, no. 9, pp. 1755–1769, Sep. 2004.

[24] T. Kailath, *Linear Systems*. Englewood Cliffs, NJ: Prentice-Hall, 1980.

[25] W. E. Arnoldi, "The principle of minimized iterations in the solution of the matrix eigenvalue problem," *Quart. Appl. Math.*, vol. 9, pp. 17–29, 1951.

[26] *Templates for the Solution of Algebraic Eigenvalue Problems: A Practical Guide*, Z. Bai, J. Demmel, J. Dongarra, A. Ruhe, and H. van der Vorst, Eds., SIAM, Philadelphia, PA, 2000.

[27] E. Chiprout and M. S. Nakhla, "Analysis of interconnects networks using complex frequency hopping (CFH)," *IEEE Trans. Comput.-Aided Des. Integr. Circuits Syst.*, vol. 14, no. 1, pp. 186–200, Feb. 1995.

[28] B. Gustavsen and A. Semlyen, "Application of vector fitting to state equation representation of transformers for simulation of electromagnetic transients," *IEEE Trans. Power Del.*, vol. 13, no. 3, pp. 834–842, Jul. 1998.

[29] E.-P. Li, E.-X. Liu, L.-W. Li, and M.-S. Leong, "A coupled efficient and systematic full-wave time-domain macromodeling and circuit simulation method for signal integrity analysis of high-speed interconnects," *IEEE Trans. Adv. Packag.*, vol. 27, no. 1, pp. 213–223, Feb. 2004.

[30] J. H. Wilkinson, *The Algebraic Eigenvalue Problem*. London, U.K.: Oxford Univ. Press, 1965.

[31] R. W. Brockett, *Finite Dimensional Linear Systems*. New York: Wiley, 1970.

[32] S. Grivet-Talocia, "Fast passivity enforcement for large and sparse macromodels," in *Proc. 13th IEEE Topical Meeting on Electrical Performance of Electronic Packaging*, Portland, OR, Oct. 25–27, 2004, pp. 247–250.
[33] R. Achar, P. K. Gunupudi, M. Nakhla, and E. Chiprout, "Passive interconnect reduction algorithm for distributed/measured networks," *IEEE Trans. Circuits Syst. II, Analog Digit. Signal Process.*, vol. 47, no. 4, pp. 287–301, Apr. 2000.
[34] V. Mehrmann and D. Watkins, "Structure-preserving methods for computing eigenpairs of large sparse skew-Hamiltonian/Hamiltonian pencils," *SIAM J. Sci. Comput.*, vol. 22, no. 6, pp. 1905–1925, 2001.
[35] G. H. Golub and C. F. van Loan, *Matrix Computations*, 3rd ed. Baltimore, MD: Johns Hopkins Univ. Press, 1996.
[36] Y. Saad, *Numerical Methods for Large Eigenvalue Problems*. New York: Halsted, 1992.
[37] ——, "Variations on Arnoldi's method for computing eigenelements of large unsymmetric matrices," *Linear Algebra Applicat.*, vol. 34, pp. 269–295, 1980.
[38] *Matlab Release 14 User's Guide*. [Online]. Available: www.mathworks.com.

Stefano Grivet-Talocia (M'98) received the Laurea and Ph.D. degrees in electronic engineering from the Polytechnic of Turin, Turin, Italy.

From 1994 to 1996, he was at NASA/Goddard Space Flight Center, Greenbelt, MD, where he worked on applications of fractal geometry and wavelet transform to the analysis and processing of geophysical time series. Currently, he is an Associate Professor of circuit theory with the Department of Electronics, Polytechnic of Turin. His current research interests are in numerical modeling of interconnects, applications of wavelets to computational electromagnetics, and passive macromodeling of lumped and distributed structures. He is the author of more than 60 journal and conference papers.

Dr. Grivet-Talocia served as Associate Editor for the IEEE TRANSACTIONS ON ELECTROMAGNETIC COMPATIBILITY from 1999 to 2001.

Andrea Ubolli received the Laurea degree in electronic engineering from the Polytechnic of Turin, Turin, Italy, in November 2003, where he is currently pursuing the Ph.D. degree.

Since graduation, he joined the EMC Group at the Department of Electronics, Polytechnic of Turin, as a Research Assistant, working on interconnect macromodeling. His research interests are in the field of electromagnetic compatibility, where he works on the macromodeling of electrical interconnects and on power integrity in micro- and macroscale complex interconnected systems.